Modelling the primary auditory cortex with a recurrent neural network and short-term synaptic depression

Dhruv Soni, Youssef Hafid, Zhi Huang Lau, Tom Roper

1. Abstract

Loebel, Nelken and Tsodyks (2007) published a model of the primary auditory cortex (A1) which was capable of replicating several biological observations of A1 neurons. In the model, an equal number of excitatory and inhibitory neurons form a column of neurons. Each of these columns represent a section of the cortex which responds most favourably to a certain frequency and are connected to several neighbouring columns. This paper aimed to replicate the results of the original model created by Loebel and colleagues, in which we recreated multiple key results such as the impact of intercortical projections on the frequency-tuning curves and the lateral inhibition effect. We also produced some novel findings related to the impact of variability in the background input to the model. We propose multiple avenues for future, including exploring long-term plasticity mechanisms and replicating biological findings on the impact of white noise on A1 neurones.

2. Introduction

In our study, we attempt to replicate a model of the primary auditory cortex (A1), which was proposed by Loebel, Nelken and Tsodyks (2007). When the model was created, a variety of nonlinear behaviours were observed within A1 through both human and animal studies. For example, it had been shown that A1 neurones show strong phasic responses to sounds and that responses to fluctuating noise can be suppressed when overlapping with sub-threshold tones of sensory input (Las et al 2005). Further investigation was unsuccessful in explaining the behaviour of these neurones though simple nonlinear neural mechanisms (Machens et al, 2004) or synaptic inhibition (Wehr and Zador, 2005). However, earlier work by Loebel and Tsodyks (2002) and Tsodyks et al (2000), achieved some success in modelling this nonlinear behaviour using a recurrent networks model. The model allowed for neural populations to work in coordination to produce population spikes (PS) of activity. The authors explored a variety of different strengths for the recurrent connections, finding that weak recurrent connectivity generated model behaviour that most closely resembled experimental findings in the A1. In the paper by Loebel et al (2007), it was hypothesized that incorporating short-term synaptic depression into the recurrent network model (Loebel and Tsodyks (2002)) could replicate the finding that A1 neurones act in coordinated ensembles of their neighbouring columns.

Their model proved robust, replicating several important experimental findings. In this paper, we look to replicate some of the findings from their original paper, as well as generating some novel results from the model. In particular, we highlight some important considerations that were not addressed in the original work, such as the effect of random seeding and background input variability. Finally, we use the results of our simulations to revisit the biological findings that it validates, originally presented by Loebel et al (2007).

3. Model and Methods

The auditory cortex model (Loebel et al (2007)) takes each auditory cortical column to be the sum of inhibitory and excitatory neurone activity, considering both recurrent and inter-column connections (Fig. 1).

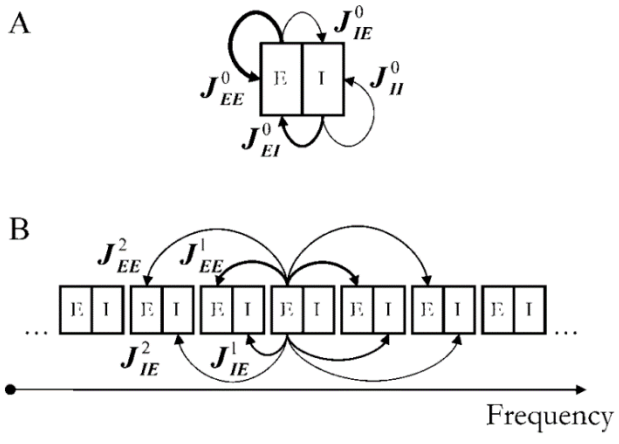

Figure 1. Diagrammatic representation of the full auditory cortex model. Each column has an excitatory and inhibitory neurone population, displaying both recurrent and intercolumn connectivity. With the synaptic strength determined by the J variables. Diagram taken from Loebel et al (2007).

The dynamics of the neurone activity were represented by a modified version of the Wilson and Cowan neural network model (1972), with each neurone having an activity-dependent decay term, as well as a firing function. For simulating multiple cortical columns, the neurone activities are represented with the following equations:

$$\tau_E \frac{dE_i^Q}{dt} = -E_i^Q + \left(1 - \tau_{\text{ref}}^E E_i^Q\right)\left[\sum_{R=-2}^{2} \frac{J_{EE}^{|R|}}{N_E} \sum_{j=1}^{N_E} U x_j^{Q+R} E_j^{Q+R} + \frac{J_{IE}}{N_I} \sum_{j=1}^{N_I} U y_j^Q I_j^Q + e_i^{E,Q} + \sum_{M=1}^{P} s_i^{Q,M}\right]^+$$

$$\tau_I \frac{dI_l^Q}{dt} = -I_l^Q + \left(1 - \tau_{\text{ref}}^I I_l^Q\right)\left[\sum_{R=-2}^{2} \frac{J_{EI}^{|R|}}{N_E} \sum_{j=1}^{N_E} E_j^{Q+R} + \frac{J_{II}}{N_I} \sum_{j=1}^{N_I} I_j + e_l^{I,Q}\right]^+$$

Where E_i and I_l represent the *i*th-excitatory and *l*th-inhibitory neurone activity, respectively. With activity referring to their firing rate, measured in Hz. $\tau_{\text{E/I}}$ is the time-constant of the system and $\tau_{ref}^{\text{E/I}}$ sets the refractory period for the neurones. The J variables describe synaptic strength, for recurrent J^0 and inter-column $J^{1/2}$ (either 1 or 2 columns distance on the tonotopic map) connections . Their subscript denotes the type of synaptic connection (for example J_{IE}^0 is inhibitory to excitatory). This notation is in-contrast to Loebel et al (2007), where J_{IE}^0 would refer to a synapse from an excitatory-inhibitory neurone. We decided to modify the notation given that it reflects the directionality of the connection better. $N_{\text{E/I}}$ refers to the number of excitatory/inhibitory neurones in the column. $e_{\text{i/l}}^{\text{E/I}}$ denotes randomized background input that the neurones are receiving, and s_i denotes the sensory input. As in Loebel et al (2007), sensory input is only delivered to excitatory neurones. The superscript Q denotes the column. The sensory input is modelled as the product of a spatial $h_i^{\text{Q,M}}$ and temporal component $\varsigma^M(t)$, as:

$$s_i^{Q,M}(t) = \zeta^M(t) h_i^{Q,M}$$

For the temporal component $\varsigma^M(t)$, this was set to match the requirements of the sensory input within a particular simulation. For example, when presenting a sustained pure tone input to a column, Cs might equal 1 when $1 \leq t \leq 2$ and 0 otherwise, where t denotes time. The spatial component, $h_i^{\text{Q,M}}$, was determined by:

$$h_i^{Q,M} = Ae^{-\frac{|Q-M|}{\lambda_S(A)}}$$

Where A is the amplitude of sensory input (Hz), M denotes the column it was presented to, which in the context of the auditory cortex, can be considered as presenting a stimulus with a frequency that column M is responds maximally to. λ_s controls the extent of the input spreading across the tonotopic map from column M to other columns. This means that even if the sensory input was not inputted to column Q, it would still receive some sensory input following an exponential decay function that depends on the distance from column Q-M and the λ_s term. λ_s was calculated as follows:

$$\lambda_S(A) = \begin{cases} \lambda_C & A \leq \alpha \\ \lambda_C + \dfrac{(A-\alpha)}{\delta} & A > \alpha \end{cases}$$

Where the spatial spread is proportional to the hyperparameter λ_c but can also be influenced by the amplitude and δ_c, if the amplitude is above a certain threshold alpha. Where δ_c determines the localization of sound input within a specific column. The influence of large (above threshold) amplitudes influencing the spread of activity were motivated by biological findings from Hudspeth (2000), who found that tuning curves from the auditory cortex are broader as sounds increase in amplitude.

The variables x_i and y_i determine the fraction of total synaptic resources that are available to facilitate the transmission, and this is further reduced by the parameter U which determines, out of this fraction, what proportion is utilized within a synaptic transmission event. The x_i and y_i variables attempt to simulate the effects of activity-dependent, short term synaptic depression, and for each neurone are dynamic according to the following equations:

$$\frac{dx_i}{dt} = \frac{1-x_i}{\tau_{rec}} - Ux_iE_i, \quad \frac{dy_l}{dt} = \frac{1-y_l}{\tau_{rec}} - Uy_lI_l.$$

Where $\tau_{rec}^{\text{E/I}}$ is the time constant for the recovery of short-term depression. To determine initial conditions for the model, we simulated it without any input and used the stabilised levels of activity and synaptic resources in each column as their starting values in other simulations. For our simulations we used a set of default parameters as in Loebel et al

(2007). Unless stated these were used across all simulations:

$$N_E, N_I = 100, P = 15, \alpha = 2, \lambda_C = 0.25, \delta_{left} = \delta_{right} = 5,$$

$$\tau_E, \tau_I = 10^{-3} \text{ second}, \tau_{rec} = 0.8 \text{ second}, \tau^E_{ref}, \tau^I_{ref} = 3 \times 10^{-3} \text{ second}$$

$$U = 0.5, e^E_1, e^I_1 = -10 \text{ Hz}, e^E_{N_E}, e^I_{N_I} = 10 \text{ Hz},$$

$$J^0_{EE} = 6,\ J^0_{EI} = 0.5,\ J^0_{IE} = -4,\ J^0_{II} = -0.5$$

$$J^1_{EI} = 3.5 \times 10^{-3},\ J^1_{EE} = 4.5 \times 10^{-2}, J^2_{EI} = 1.5 \times 10^{-3},\ J^2_{EE} = 1.5 \times 10^{-2}$$

To demonstrate model behaviour for a single column, we simulated the population response of a column to a pure tone of sensory input (Fig. 2). As can be seen, the column exhibits a sharp non-linear spike following the tone onset and displays no further spiking despite the sensory input persisting. At a population level, this signifies the synchronised activity of the excitatory neurones increasing at the same time, followed by the coordinated activity of the inhibitory neurones to bring the activity back down to baseline.

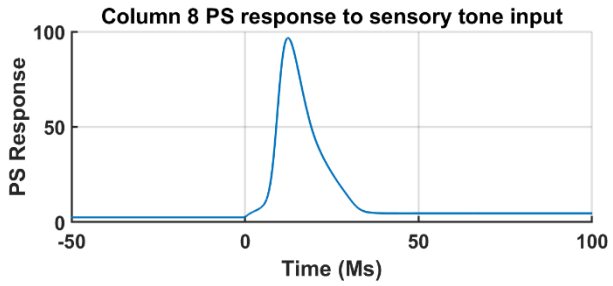

Figure 2. Population spike response in a single column. Pure tone sensory input is delivered to the column ($A = 4$) at 0ms for the duration of the simulation.

To generate randomized background input, we drew numbers from a uniform distribution that ranged from –10 to 10. Our simulations were undertaken in MATLAB with a random seed of 33. In Loebel et al (2007), the impact of this random variability on the model behaviour was not explored. We decided to investigate this in Fig. 3 by monitoring how the max response from Fig. 2 changes as a function of the random seed.

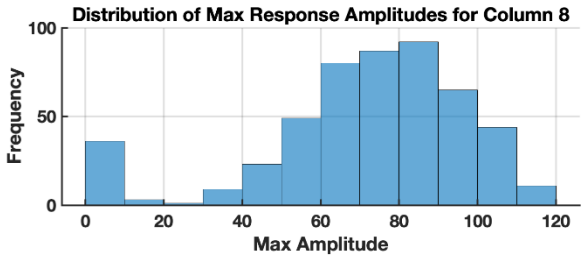

Figure 3. Response variability due to random seeding. We present novel findings from 500 realizations of a pure tone input at column 8 (A=4), showing a wide range of variability in the distribution of maximum responses in column 8. Including some realizations where a PS response is absent.

After repeating this for 500 seeds we note that simply changing the random draw of numbers is sufficient to completely change the behaviour of the model, with the column varying in its average response to sensory input between roughly 40 and 120hz, and in some instances being completely absent of a PS response. This refers to the furthest left bin, which was below our defined threshold for a PS (see Fig. 5). Due to only 100 excitatory and inhibitory neurones being in each column, the random variability has a much bigger impact on the overall level of background input the columns receive, and therefore how many neurones receive sensory input. This variability in response is overcome by increasing the number of neurones in each column (Fig. 4), and we return to this point in our discussion.

For the rest of the paper, we simulated that the randomized background input ($e^{E/I}_{i/l}$) was identical across each column, which was our interpretation of the methods followed Loebel et al (2007). While their methodology for this feature was not explicit, we felt this was suitable, as using different background inputs for each column caused asymmetries in the spread of PS activity across the tonotopic map that weren't seen in the original paper (Fig. 4).

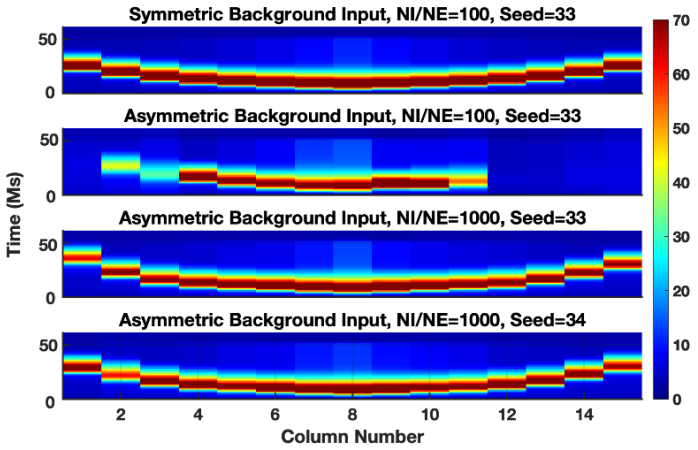

Figure 4. Impact of neurone magnitude and randomization on the symmetry of PS spread between columns. We generate novel findings that the effect of background input varying across columns causes an asymmetric spread of PS activity (panel 2) despite getting the same sensory input as panel 1. Increasing the number of neurones in each column can almost restore the symmetry of PS activity and is robust across realizations (panels 3 and 4). Sensory input is identical to Fig. 2.

Whether each column receiving the same background input is biologically plausible remains something that we would explore in future work. We did, however, explore the impact of this decision on the model results. As can be seen in Fig. 4, when the background input is identical across columns, sensory input into column 8 has a symmetric spread (1st panel), however, when background input is random across columns this leads to an asymmetric response (2nd panel). This was caused by the small number of overall neurones used (100 excitatory and inhibitory) causing noticeable variation in background input between columns, influencing their relative drive as well as how much sensory input they would receive from an input. Using a small number of neurones matched the original model in Loebel et al (2007), but also reflected the limitations of our computational capabilities. Despite having to set a strict constraint on our model, that background input should be equal across columns, this might reflect the limitation of only using 100 of each neurone type within a column. In Fig.4 (3rd and 4th panel) we simulate the effect of using different background inputs for each column, but with much larger levels of neurones (1000 of E and I). In this instance, the symmetry of the PS activity is almost fully restored, with PS activity reaching to the boundary columns 1 and 15, and this is robust across two different realisations of the randomised background input. In the brain, there is evidence to suggest that neurones in cortical columns are more likely to be in the order of thousands (Mountcastle, 1997) rather than 100's. Therefore if, in reality, background input should be different for each column, the scale of neurones might make the individual differences in background input between columns unnoticeable. Therefore, in the case of only simulating 100 neurones, setting the background inputs equal in each column could act as a suitable approximation for what we might expect in reality.

In most simulations we recorded responses of the model as population spikes, which was the average activity of all excitatory neurones within an auditory column. Typically, we found that population spikes were elicited whenever a column's excitatory activity reached a certain level of activity, as after this point a sharp non-linear increase in the maximum excitatory response is witnessed (Fig. 5). We used plots like these to understand the minimum amplitude of sensory input that was required to elicit a PS response, of which we typically looked at a threshold of 20 to identify a PS. Supplementary to our results in Fig. 3, we also found that different realizations of the amplitude-response curves uncovered that the effect of randomisation can impact the threshold of the PS response (shifting curve along x-axis) as well as the maximum response possible from the column (changing plateau of max response).

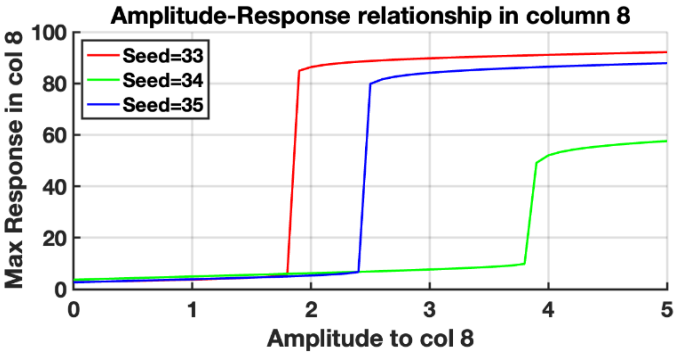

Figure 5. Non-linear amplitude-response curve for column 8, also dependent on realisation. Novel results showing the max PS response of column 8 for changes in input amplitude. Different realizations can change the amplitude-response relationship, causing a shift of the curve, as well as changing its peak plateau of maximum response.

4. Results

4.1 Basic Behaviour

To demonstrate the behaviour of the full model we input a pure tone of sensory input into column 8, lasting for 200ms. We recorded the PS response of columns in the region of 8 as a function of time (Fig. 6a). A population spike is elicited in column 8 as well as 9 and 7, despite the input targeting column 8. Columns 10 and 6 display some increases in mean excitatory activity in response to the sensory input, but it is insufficient to produce a population spike response. We also plotted the total sensory input that was received by each column (figure 5b), which demonstrates the spatial spread of sensory input to neighbouring columns of the input column (8).

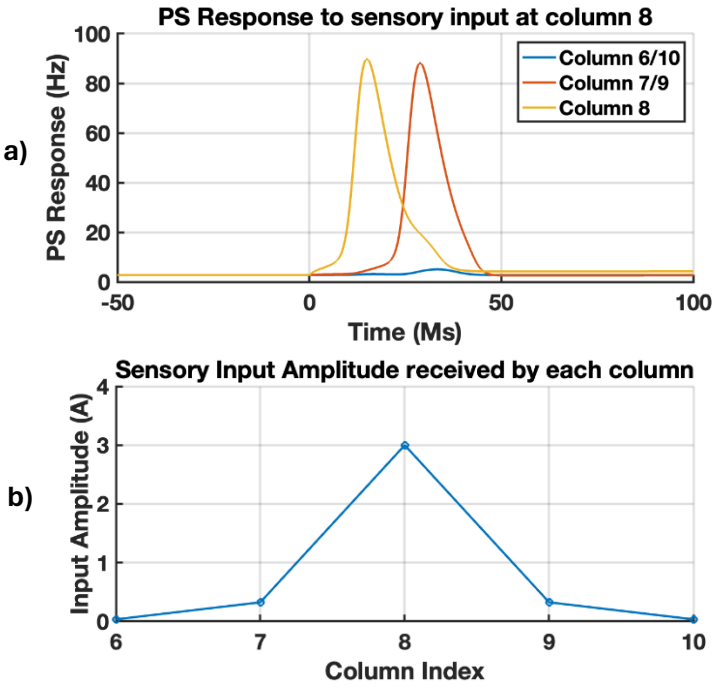

Figure 6. PS responses to pure tone input at column 8. A) Population activity for columns 6-10 for sustained input (A=4) at column 8 from t=0. **B)** Sensory input amplitude received by each column.

We next looked to demonstrate how sensory input can cause PS activity that dynamically spreads across the columns in the model. Fig. 7 shows a heatmap visualisation of the simulations shown in Fig. 6, but instead recording PS activity from all columns, and in response to varying amplitudes of input. The bottom panel represents the smallest amplitude and increases until the maximum amplitude in the top panel (ranging from 2-14Hz). The colour map highlights the gradation of PS spread, where lower amplitude inputs result in more confined activation patterns. For example, with an amplitude of 2, not even column 8 exhibits a PS, but with an amplitude of 15 all columns in the model show PS responses. Higher amplitudes also lead to a faster spread of activity, which corresponds to a flatter shape of the PS spread across columns.

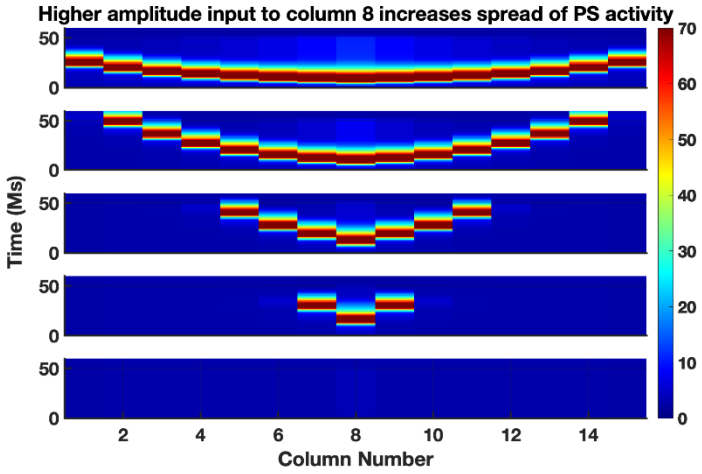

Figure 7. Degree and speed of spread across columns depends on input amplitude PS responses across all columns plotted for a variety of amplitudes from weakest (bottom panel) to strongest (top panel). Amplitudes were 2, 4, 6, 11 and 15. Timing of sensory input is identical to Fig. 6.

To further understand the behaviour driving the PS activity, we plotted the response of excitatory and inhibitory neurone populations in column 8 to a weak and strong sensory input (Fig. 8). Using a smaller amplitude caused a longer delay before the PS response is elicited (response curve is shifted to the right), but in both cases the responses of both neurone types are synchronized. In similarity to the original paper (Loebel et al (2007)), we saw that excitatory neurons display quicker onsets of activity, always increasing in activity in response to the stimulus onset, however the inhibitory neurone population only shows activity changes in response to the excitatory PS. The fact that both populations show coordinated activity across different amplitudes of input makes sense, as the inhibitory population would be required to keep the excitatory activity within

reasonable bounds, maintaining the dynamic balance that can facilitate a PS.

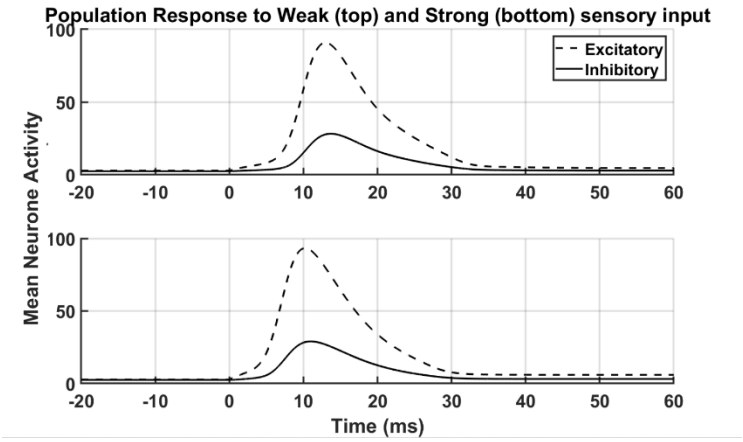

Figure 8. Stronger input gives faster responses. Population responses of excitatory and inhibitory neurones in column 8 to a weak (A=3.7, top panel) and strong (A=6, bottom panel) input, presented as a pure tone to column 8, starting at t=0.

We next quantified the relationship between the input amplitude and the PS response latencies. Fig. 9, shows the latencies from sensory input to a PS response in columns 8, 10 and 12 for a stimulus presented to column 8. As the amplitude of the auditory stimulus increases, the latency of responses in all three columns decreases and levels off. This matches our results from Fig. 7, where increased input amplitudes were met with a faster onset to PS in column 8, as well as a flatter spread of activity across columns, indicating that the PS was transferring to other columns faster.

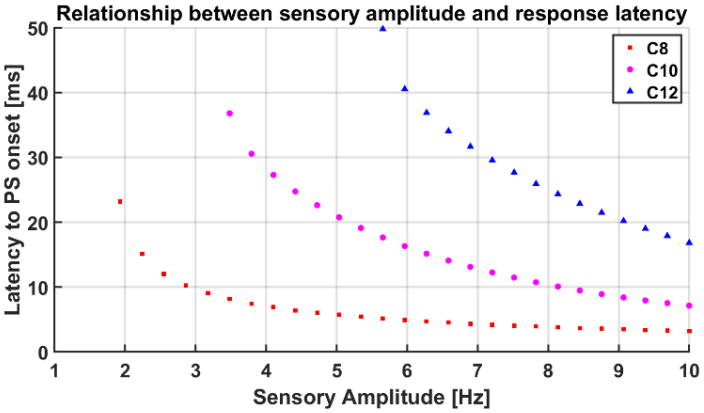

Figure 9. Amplitude of sensory input influences latency to onset of PS response. Sensory input at different amplitudes were presented to column 8 as a pure tone from t=0, and latencies to onset of PS responses in columns 8, 10 and 12 were plotted.

4.2 Frequency Tuning Curves

Next, we looked to recreate the frequency tuning curves (FTC) that were presented in the original paper. Frequency tuning curves show the minimum strength of a stimulus needed to elicit a response at a certain column. This was achieved by inserting sensory tones of various amplitudes and columns for 50ms and recording the minimum amplitude required to elicit a PS within column 8 (Fig. 10a). This results in a V-shaped curve, where a higher stimulus amplitude is needed to elicit a PS in column 8 if the distance between column 8 and the targeted column is larger. Similar to the original paper (Loebel et al (2007)), we found that manipulations of several parameters would result in changes to the FTC that are consistent with studies—of A1 cortex. For example, when connections between the columns were absent (changing the strength of the inter-column connections $J^{1/2}$ to 0), the FTC became narrower (Fig. 10a). For sensory input to any column that was not 8, the amplitude needed to elicit a PS increased. This is because without the connections, columns are rendered incapable of sending excitatory signals to its neighbours, thus reducing the amount of excitatory input received by those neighbouring columns.

Manipulating the recurrent inhibition resulted in similar FTCs to those in the original paper (Fig. 10b). Reducing the inhibition reduced the threshold needed for a PS to occur while increasing the inhibition required a higher amplitude to elicit a PS. Increasing the delta value for just one of the sides creates an asymmetric spread of the sensory inputs. The simulation of this current model was consistent with the original paper (Fig. 10c), as when the delta value was increased, the threshold needed to elicit a PS at column 8 also increased. This reflected that sensory input would spread less favourably to columns on the left of the input column.

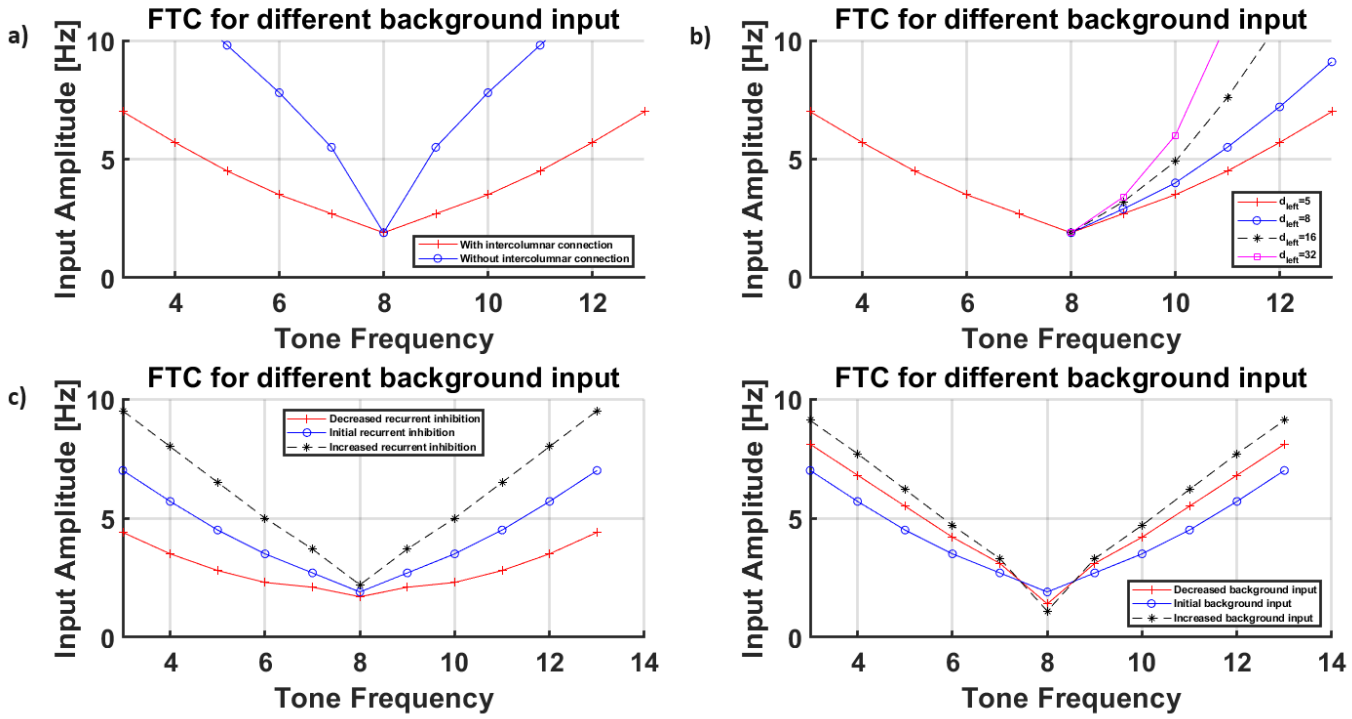

Figure 10. Frequency Tuning Curves for four different scenarios A) Removing intercolumnar connections resulted in reduced range of frequencies eliciting spiking behaviour (a sharper tuning curve) across the range of amplitudes, as well as a general increase in minimum amplitude to elicit PS in all columns other than column 8 **B)** Asymmetric stimuli spread results in an asymmetric FTC **C)** Lower levels of recurrent inhibitory activity requires weaker stimuli to elicit PS **D)** Alter the strength of background inputs results in varying shapes of FTCs.

A1 neurons receive input from other brain regions as well, not just auditory stimuli, and this is represented in this model as background input. After increasing the amount of background input that is going into each neuron, the neuron would have less available resources for auditory input and therefore would need a stronger stimulus to elicit a PS, resulting in a narrower tuning curve as shown in Fig. 10d. The manipulation of the amount of background input was done by adding or subtract a certain value from the inputs (e_i^E and e_i^I), which in this paper was 2. However, a point of divergence to the original paper was then even though reducing the amount of background input resulted in a wider tuning curve that had a lower threshold compared to when background input was increased, the thresholds were still higher than when there was no change in background input. Furthermore, when altering the background input by larger margins, the threshold is increased regardless of direction, and this could be an interesting direction to conduct further investigation.

4.3 Effect of Masking

Forwards masking occurs when the presentation of a stimulus suppresses the response a subsequent stimulus for a short period of time, which is about several hundred milliseconds in A1 (Brosch and Schreiner, 1997; Calford and Semple, 1995). In this model this effect is caused by a depletion of synaptic resources, or short-term depression. We input pairs of sensory stimuli to column 8, for different interstimulus intervals and plot the masker PS as well as the probe PS (Fig. 11a). As can be seen, for shorter ISIs the response to the probe is much smaller than the maker stimulus. As the ISI increases it recovers in magnitude the response of column 8 to the second input of each pair (Fig. 11a). The first input in each pair is referred to as the 'masking' stimulus and the second as the 'probe' stimulus.

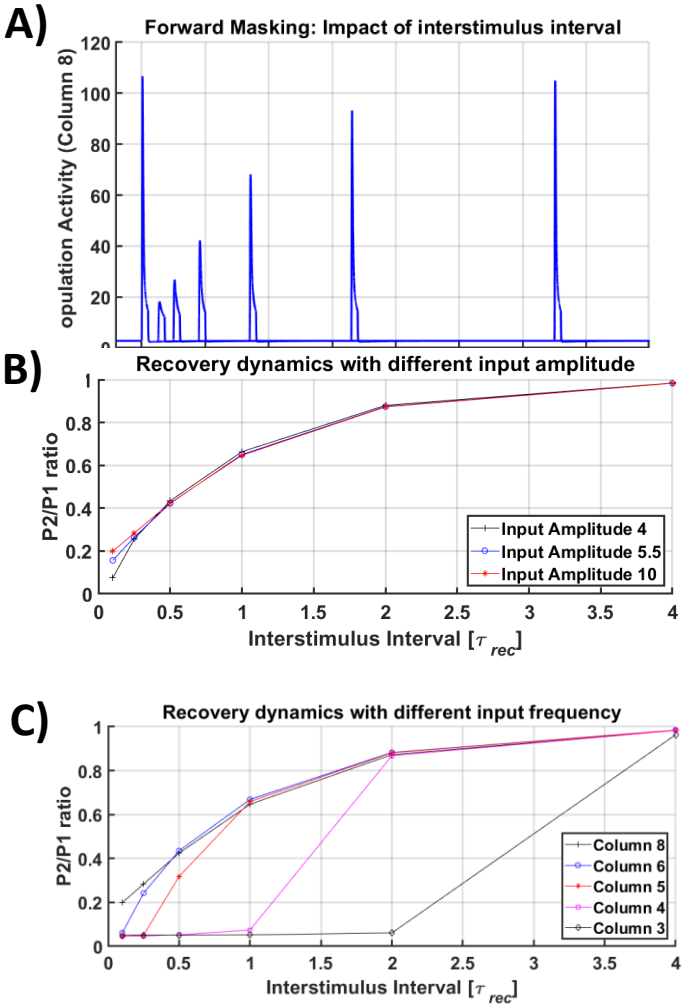

Figure 11. Response dynamics of masking. A) Spike recovery in column 8: First spike is response to the mask, subsequent spikes are the responses to probes that are presented at varying time intervals from the initial mask. Max response to the probe is only restored with interstimulus intervals are beyond 3000ms **B) Recovery dynamics for different input amplitudes** When the interstimulus interval between the masker and the probe is short, the amplitude of the PS elicited by the probe is significantly smaller compared to when the interstimulus interval is long, as illustrated in Figure 6a. **C) Recovery dynamics with different input columns** When the distance between the tone pairs are further away from the measured column (Column 8), the time needed for PS to recover is longer.

Next, we investigated whether the strength of the inputs would influence the recovery dynamics of the PS (Fig. 11b). The P2/P1 ratio was calculated by dividing the peak response of the probe by the peak response to the masker. Like the original paper, we found minimal effect of input amplitude on how spikes recover as ISI increases. We were also able to replicate the effect of tone pair frequency on recovery dynamics as shown in the original paper. The further away the column corresponding to the frequency of the tone pairs to the observed column, which is column 8, the slower the recovery dynamics and the longer the interstimulus interval needed for the probe to elicit a PS.

We next looked to investigate the impact of masking on the spread of PS activity throughout the cortical columns, as well as relating this to the recovery time of the neurones (Fig. 12). This figure shows the reduced responsiveness to the probe following a mask, and the time dependency of the masking inhibition. The longer the Inter-Stimulus Interval (ISI) the lower the inhibition of the PS spread. This long-lasting inhibition of spread extended well beyond $\tau_{rec}^{E/I}$ (time constant of the short-term depression process). This aligns with the results of the original paper, which modelled both forward masking as well as its time dependence. These are already well established in the literature. Brosch and Schreiner (1997) were able to experimentally observe forward masking within cat neurones ranging from 53-430ms, in our own results, forward masking extended far longer, still observable with an ISI well over 1000ms (Fig. 12).

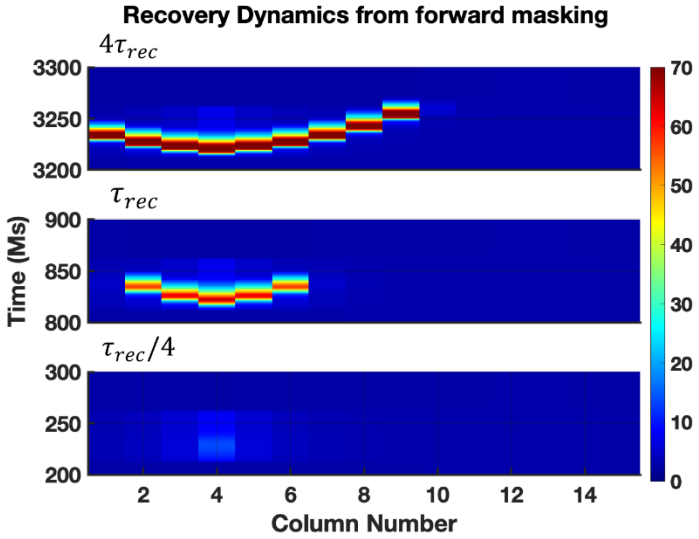

Figure 12. Impaired PS spread due to forward masking outlasts the timescale of short-term depression. In each panel a pair of 10 Hz stimuli are presented to column 4. Three different ISI's were used: $\tau_{rec}/4$ (bottom panel), τ_{rec} (middle), and $4\tau_{rec}$ (top panel). A=8 for both stimuli, duration of input was 10ms and 50ms for masker and probe, respectively. Masker was presented at t=0.

To understand the relationship between the degree of response to the probe and the interstimulus interval, we next looked to plot FTCs for different ISI's (Fig. 13). This followed the same procedure as Fig. 10 but (for the coloured lines) we consider the minimum amplitude required to get a PS response for the probe stimulus. We demonstrated that decreasing the ISIs caused a sharpening of the tuning curve, which meant that the minimum amplitude required to produce a PS response to the probe stimulus was higher as the ISI decreased. This is expected given the previous results showing that subsequent responses to a stimulus of equal amplitude are smaller when ISIs are shorter.

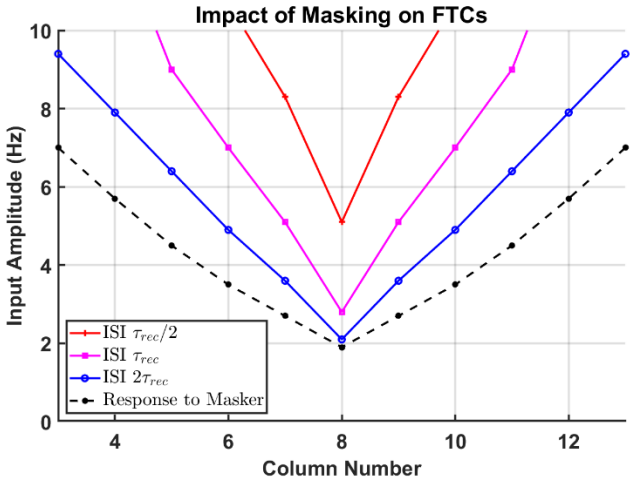

Figure 13. Impact of masking and ISIs on the FTC of column 8 Black dashed line is the normal FTC for column 8 (as in Fig. 10), coloured lines correspond to FTCs for the probe stimulus to produce a PS response in column 8.

To conclude our investigation of masking, we looked at the impact of the spatial location of the masking input. We input tones with frequencies ranging from columns 1-15 as the masker while the probe frequency was always set at column 8 (Fig. 14). The amplitude of the masker was set to be 4Hz. The amplitude of the probe was set to be capable of eliciting a PS if inserted individually (2Hz). Due to the short ISI, when a PS is elicited by the masker, no PS will be elicited by the probe as there is not enough time for the resources to recover. Identical to the original paper, for maskers with the frequency of columns 5 and 11, even though there is no PS elicited by the masker, there is no PS elicited by the probe. Despite the maskers not being strong enough to elicit a PS in column 8, they still used up some of the synaptic resources, which must have been sufficient enough to inhibit the probe response.

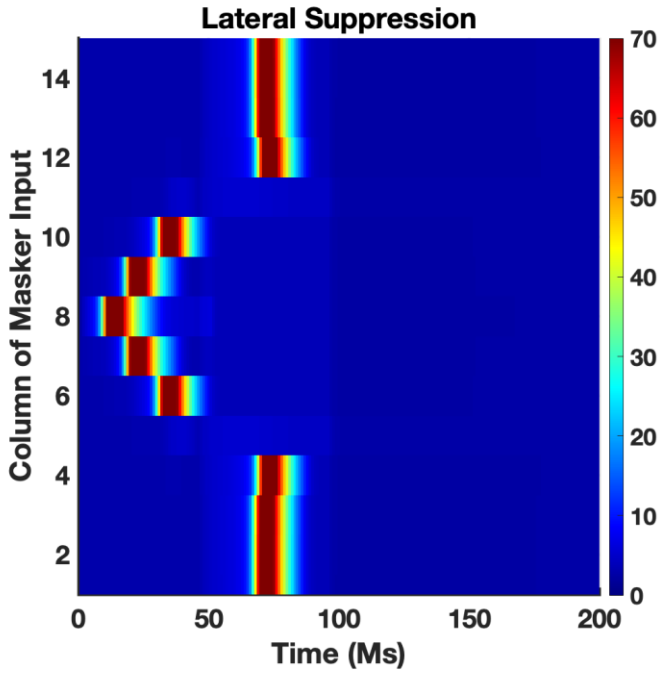

Figure 14. Lateral suppression effect. Responses of column 8 to a probe inserted into its own column, after a masker is presented to columns from 1-15. First pattern of response corresponds to the masker (A=4) and second to the probe (A=2). In column 11 and 5, response was absent to both stimuli. Masker was from 0-50ms, probe was 45-90ms.

4.4 Complex Sound

Finally, we sought to investigate the impact of more complex sounds on the auditory cortex model, given that most sounds up to this point have been relatively simple. We plot the PS responses of all columns in Fig. 15a showing the response to multiple sensory inputs, targeting different columns at different times and input amplitudes. The interaction between many overlapping inputs can be seen to produce almost no PS response within column 4 just before 600ms into the simulation. This corresponds to the brown, yellow and light blue blocks in Fig. 15b, from roughly 500-700ms. Interestingly, this absence of a large PS response is the case even though one of the inputs is a high amplitude (A=8, brown block), and the same amplitude input can produce a normal PS response later in the simulation (last brown block, inputted to column 8 in Fig. 15b).

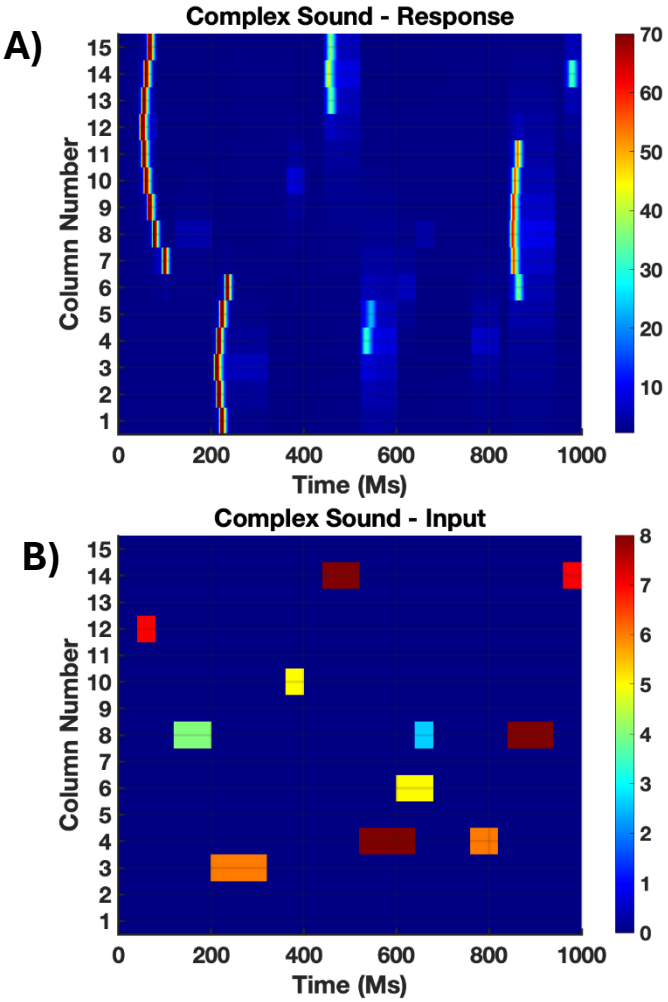

Figure 15. Response of the model to a complex sound a) Complex Sound - Response PS activity of columns in response to the complex input **b) Complex Sound - Input** Each block represents a single sensory input, with colours representing the input amplitude

5. Discussion

In this paper, were able to replicate most features of the original model proposed by Loebel et al (2007). Furthermore, some features have been linked to key biological findings of the auditory cortex which we summarise in Table 1.

Experimental observation	References	Figure
Temporal ordering of inhibitory and excitatory cortical responses; Co-tuning of excitation and inhibition	Wehr and Zador (2003), Zhang et al. (2003), Las et al. (2005)	Figure 8
Frequency tuning curves (FTC)	Kilgard and Merzenich (1999), Shreiner et al. (2000)	Figure 10
Dependency of FTC bandwidth on intracortical connectivity	Kauret al. (2004)	Figure 10a
Dependency of FTC bandwidth and threshold on cortical inhibition	Chen and Jen (2000), Wang et al. (2002)	Figure 10c
Forward Masking: recovery dynamics	Calford and Semple (1995), Brosch and Schreiner (1997), Wehr and Zador (2005)	Figure 11
'Lateral Inhibition - Response to stimulus in a column is inhibited by prior activation in a neighbouring column	Shamma et al. (1993), Rotman et al. (2001)	Figure 14

Table 1: Recreated Findings on A1 Neuronal Response Characteristics as Reproduced by Our Model (Adapted from Loebel et al (2007))

For example, the model demonstrated the dependency of FTCs on the intercolumn connectivity and levels of inhibition (Fig. 9), recreated the process of lateral inhibition (Fig. 13) and shows the precise co-tuned responses of the inhibitory populations to the excitatory PS (Fig. 7). We also generated some novel results, such as the impact of the random nature of the background input and how this can produce significantly different results across realisations, especially with small numbers of neurones in each column (Fig. 2,3,4). There were certain modelling decisions that we replicated here for sake of consistency, but that we would look to address in future work. One consideration relates to the use of only 100 excitatory and inhibitory neurones in each column. We investigated the impact of using a larger number of neurones and whether this allowed us to simulate the more biologically plausible case that all columns received different sets of background input. It would be important to see whether we could simulate other key findings within this paper at a larger neurone count and with background input varying across columns. One important consideration that was not explored here concerns boundary conditions of the tonotopic map. Given that all columns are receiving input from their two closest neighbours, this implies that columns 1-2 and 14-15 will not be receiving similar levels of intercolumn input as the other columns. It would be important to explore

whether these boundary columns receive less input from spreading PS activity. If this is the case, we would expect this to also be a finding from biological experiments, If not, this might suggest that the reduction in drive for boundary columns is overcome by having stronger intercolumn connections between their existing neighbours. This could be explored by adjusting the synaptic weights of boundary columns in this network model.

Another point that we would like to investigate is the decision to only provide sensory input to excitatory neurones. In our replication of the model, we followed this procedure based on the original descriptions by Loebel et al (2007). However, there is evidence that the auditory thalamus has connections to A1 interneurons. As the auditory thalamus is a necessary component of the auditory pathway, this leads to the possibility that some A1 inhibitory neurones will be receiving sensory input (Studer and Barkat, 2022). The model also lacks any form of long-term plasticity, despite incorporating short-term mechanisms. Kudoh & Shibuki (1994) have shown that long-term potentiation mechanisms are present from *in vitro* experiments of the rat auditory cortex, what these mechanisms are driving and their implementation in this model could be investigated.

The model also provides a potential explanation for the finding that low-level white noise has been found to enhance frequency discrimination in mice (Christensen et al 2019). Though not a perfect model, increasing background stimulation might represent a similar effect to the white noise, given that it's a random input and covers all auditory frequencies (represented as columns in our model). When we increased background stimulation, a sharpening of the tuning frequencies occurred (Fig. 10d). This finding corroborated with Christensen's results; that white noise leads to widespread inhibition and the sharpening of tuning curves in the auditory cortex. A better method to model their findings would be to use white noise as input to our model, rather than increasing background noise. For example, we could input sensory stimuli across all columns, at a low and random amplitude, to simulate this effect This method would better distinguish the effects of natural background stimulation and white noise.

Furthermore, Rothschild et al (2009) found that in A1 cortical columns, feedforward connections are found in the middle layers, but recurrency is only witnessed in superficial and deeper layers. Whether explicitly considering this layer dependent connectivity would make a difference to the model behaviour should be explored. Elucidating the function of network recurrence would be a good exploratory step in investigating this. The model we used is only for A1 neurones, the first layer to receive input, so would be most suitable for investigating the role of early recurrence. Studying the mice auditory cortex, Aponte et al (2021) found that the recurrence plays a significant role in direction sensitivity in A1 neurones (whether a sound is increasing or decreasing in frequency), with inhibition of interneurons in recurrent circuits reducing disparity between responses to upwards and downwards shifting stimuli. To attempt to model this, we could simulate neural populations that have varying directional sensitivity. Using frequency sweeps (stimuli from low frequency to high, or vice versa) it would be possible to observe differences in response based on directionality. Then, by changing the strength of the recurrent connections in our network, we could observe any changes to the selectivity of the neurones.

Finally, our model has an implied tonotopic arrangement, with neighbouring columns or A1 regions responding to similar frequencies of input. This is because sensory input of a preferred frequency for column M, will also be favoured by its neighbouring columns, and the spatial spread of the input will reflect this. However, within the auditory cortex there is evidence to suggest that the tonotopic map is arranged differently, with regions that respond preferably to low tones being bordered on either side by high tone regions (Costa et al, 2011). Therefore, replicating this structure might result in a model more representative of the dynamics in the auditory cortex.

6.Contributions

The authors confirm the contributions to the paper as follows:

Methodology: Dhruv Soni, Youssef Hafid, Zhi Huang Lau, Tom Roper;

Software: Dhruv Soni, Youssef Hafid, Zhi Huang Lau, Tom Roper;

Investigation, Dhruv Soni, Youssef Hafid, Zhi Huang Lau, Tom Roper;

Visualization, Dhruv Soni, Youssef Hafid, Zhi Huang Lau, Tom Roper;
Writing: Dhruv Soni, Youssef Hafid, Zhi Huang Lau, Tom Roper.
Supervision: Markus Owen

6. References

Aponte, D. A., Handy, G., Kline, A. M., Tsukano, H., Doiron, B., & Kato, H. (2021). Nature Communications, 12(1).

Brosch, M. and Schreiner, C.E. (1997) Journal of Neurophysiology, 77, pp. 923-943.

Calford, M.B. and Semple, M.N. (1995) Journal of Neurophysiology, 73, pp. 1876-1897. Neuropsychologia, 117, pp. 102-112.

Chen, Q.C. and Jen, P.H. (2000) Hearing Research, 150, pp. 161-174.

Christensen, R.K., Lindén, H., Nakamura, M. and Barkat, T.R. (2019) Cell Reports, 29(7), pp. 2041-2053.

Costa, S., Zwaag, W., Marques, J., Frackowiak, R, Clarke, S., Saenz, M. (2011) Journal of Neuroscience, 31 (40), pp. 14067-14075

Crasta, J.E., Thaut, M.H., Anderson, C.W., Davies, P.L. and Gavin, W.J. (2018)

DeWeese, M.R., Wehr, M. and Zador, A.M. (2003) Journal of Neuroscience, 23, pp. 7940-7949.

Kaur, S., Lazar, R. and Metherate, R. (2004) Journal of Neurophysiology, 91, pp. 2551-2567.

Kilgard, M.P. and Merzenich, M.M. (1999) Hearing Research, 134, pp. 16-28.

Las, L., Stern, E.A. and Nelken, I. (2005) Journal of Neuroscience, 25, pp. 1503-1513.

Loebel, A., Nelken, I., and Tsodyks, M. (2007) Frontiers in Neuroscience, 1, pp. 197-209, November.

Masaharu Kudoh, Katsuei Shibuki, Neuroscience Letters, Volume 171, Issues 1–2,1994, Pages 21-23, ISSN 0304-3940

Rothschild, G., Nelken, I. & Mizrahi, A. Nat Neurosci 13, 353–360 (2010).

Rotman, Y., Bar-Yosef, O., and Nelken, I. (2001). Relating cluster and population responses to natural sounds and tonal stimuli in cat primary auditory cortex. Hear. Res. 152, 110 127.

Schreiner, C.E., Read, H.L. and Sutter, M.L. (2000) Annual Review of Neuroscience, 23, pp. 501-529.

Shamma, S. A., Fleshman, J. W., Wiser, P. R., and Versnel, H. (1993). Organization response areas in ferret primary auditory cortex. J. Neurophysiol. 69, 367–383.

Studer, F. and Barkat, T.R. (2022) Neuroscience & Biobehavioral Reviews, 132, pp. 61-75.

V B Mountcastle, *Brain*, Volume 120, Issue 4, Apr 1997, Pages 701–722.

Wang, J., McFadden, S.L., Caspary, D. and Salvi, R. (2002) Brain Research, 944, pp. 219-231.

Wehr, M., and Zador, A. M. (2003). Balanced inhibition underlies tuning and sharpens spike timing in auditory cortex. Nature 426, 442–446.

Yin, P., Johnson, J.S., O'Connor, K.N. and Sutter, M.L. (2011) Journal of Neurophysiology, 105(2), pp. 582-600.

Zhang, L.I., Tan, A.Y.Y., Schreiner, C.E. and Merzenich, M.M. (2003) Nature, 424, pp. 201 205.